

1 **Zero-dimensional transient model of large-scale cooling** 2 **ponds using well-mixed approach**

3

4 Ahmed Ramadan^{1*}, Reaz Hasan², Roger Penlington³

5 ^{1,2,3} Northumbria University at Newcastle, Department of Mechanical and Construction
6 Engineering, Newcastle upon Tyne, NE1 8ST, UK.

7 * corresponding author: Ahmed Ramadan: Fax: +44 191 232 6002 E-mail address:
8 ahmed.ramadan@northumbria.ac.uk

9

10 **Abstract**

11 Nowadays, nuclear power plants around the world produce vast amounts of spent fuel. After
12 discharge, it requires adequate cooling to prevent radioactive materials being released into the
13 environment. One of the systems available to provide such cooling is the spent fuel cooling
14 pond. The recent incident at Fukushima, Japan shows that these cooling ponds are associated
15 with safety concerns and scientific studies are required to analyse their thermal performance.
16 However, the modelling of spent fuel cooling ponds can be very challenging. Due to their large
17 size and the complex phenomena of heat and mass transfer involved in such systems. In the
18 present study, we have developed a zero-dimensional (Z-D) model based on the well-mixed
19 approach for a large-scale cooling pond. This model requires low computational time compared
20 with other methods such as computational fluid dynamics (CFD) but gives reasonable results
21 are key performance data. This Z-D model takes into account the heat transfer processes taking
22 place within the water body and the volume of humid air above its surface as well as the
23 ventilation system. The methodology of the Z-D model was validated against data collected
24 from existing cooling ponds. A number of studies are conducted considering normal operating
25 conditions as well as in a loss of cooling scenario. Moreover, a discussion of the implications
26 of the assumption to neglect heat loss from the water surface in the context of large-scale ponds
27 is also presented. Also, a sensitivity study is performed to examine the effect of weather
28 conditions on pond performance.

29 **Keywords:** Spent nuclear fuel, large-scale cooling ponds, analytical modelling, well-mixed
 30 approach, transient heat transfer.

Nomenclature			
A	surface area (m ²)	y	mole fractions
C_p	specific heat capacity at constant pressure (J/kg K)	Δt	time step size (s)
C_w	specific heat capacity of water (J/kg K)	<i>Greek symbols</i>	
h_c	convection heat transfer coefficient (W/m ² K)	ε	emissivity
h_{con}	condensation mass transfer coefficient (m/s)	ρ	density (kg/m ³)
h_{ev}	evaporation mass transfer coefficient (m/s)	σ	Stefan-Boltzmann constant (W/m ² K ⁴)
$h_v(T)$	enthalpy of vapour at a given temperature (kJ/kg)	<i>Subscripts</i>	
h_{fg}	latent heat of vaporisation for water (kJ/kg)	a	dry air
k	thermal conductivity (W/m K)	∞	ambient
m	mass (kg)	c	convection
\dot{m}	mass flow rate (kg/s)	con	condensation
M	molecular weight (kg/kmol)	d	heat load
N	mole number (kmol)	D	designed value
\dot{N}	molar flow rate (kmol/s)	ev	Evaporation
Nu	Nusselt number	h	hall
P	pressure (Pa)	l	leakage
\dot{Q}	heat transfer rate (W)	m	make-up
Ra	Rayleigh number	p	pond
RH	relative humidity (%)	r	radiation
R_o	universal gas constant (J/K kmol)	R	rack
Sh	Sherwood number	sat	saturation
T	temperature (K)	t	total
V	Volume (m ³)	v	vapour
x	wall thickness (m)	$vent$	ventilation
		w	water
		wb	wet bulb

31 **1 Introduction**

32 In the past decades, increasing the use of nuclear power for electricity generation has gained a
33 lot of attention amongst scientists. Nuclear reactors around the world are now discharging a
34 massive amount of spent nuclear fuel, which is predicted to reach approximately 445,000 t HM
35 (metric tonnes of heavy metal) by 2020 [1]. This includes 69,000 t in Europe and 60,000 t in
36 North America. Despite the recent incident at Fukushima, Japan [2], nuclear power generation
37 continue to grow in developed countries, as evidenced by the recent massive investment in
38 nuclear energy by the UK government in approving an £18bn nuclear plant at Hinkley Point
39 C. This will deliver 7% of Britain's electricity needs for the next six decades [3].

40 The issue of long-term storage was not considered when the original decisions were made
41 regarding the fuel cycle [4]. Recently, waste management has become one of the major policy
42 issues in most nuclear power programmes. Meanwhile, the options chosen for waste
43 management can have extensive effects on political debates, propagation risks, environmental
44 threats, and economic costs of the nuclear fuel cycle. This increases the significance of
45 modelling the cooling ponds and analysing their performance to provide a better understanding
46 of their pond thermal behaviour. This will allow for better operation and could offer mitigation
47 options whenever needed in accident scenarios.

48 Several research investigations have considered the thermal-hydraulic behaviour of the spent
49 fuel cooling ponds, which are mainly focused on accident scenarios and their consequences [2,
50 5-8]. These studies used two main modelling approaches. The first approach is the use of so-
51 called system codes such as RELAP, TRACE, ATHLET, MELCOR and ASTEC. These codes
52 are based on dividing the system into a network of pipes, pumps, vessels, and heat exchangers.
53 Mass, momentum and energy conservation equations are then solved in one-dimensional form.
54 Many phenomena and physical behaviour such as two-phase flows and pressure drop due to
55 friction rely on empirical correlations. These codes are suitable for systems that can be
56 represented by one-dimensional flows. However, when such a system involves multi-
57 dimensional phenomena, these codes do not provide a good approximation. Some attempts
58 have been made to improve their capability to handle multi-dimensional flows. One of these
59 attempts considers the system as an array of parallel one-dimensional pipes, where the
60 interaction between them is allowed through cross-flow coupling. Although they provide
61 improved approximations compared with purely one-dimensional approaches, these models do

62 not offer appropriate descriptions of multi-dimensional flows. The MARS code is an example
63 of attempts to include a multi-dimensional analysis capability in system codes [9].

64 The second approach is a numerical method such as computational fluid dynamics (CFD)
65 which in principle can address details of thermos-fluid phenomena in cooling ponds. Numerical
66 methods such as CFD can be used, in principle, to address fluid flow and heat transfer scenarios
67 in three dimensions using computers. The CFD methodology is now well-established, but the
68 available literature indicates that a full CFD model of a spent fuel cooling pond may be not
69 practically possible. This is due to their large size and the existence of complex phenomena,
70 such as evaporation, which requires multiphase flow models. However, some studies have
71 reported CFD modelling of spent fuel ponds taking into account only the water body without
72 considering the humid air zone above or ventilation and their effect on the evaporation rate.
73 Also, some of the challenges encountered during the CFD simulation have been discussed in
74 our previous work [10]. An example of the use of CFD in improving the safety of such cooling
75 ponds can be found in a study conducted by Ye et al. [11], in which a new passive cooling
76 system was designed to provide an adequate cooling for the CAP1400 spent fuel pool in
77 emergency situations. Hung et al. [12] used the CFD approach to predict the cooling ability of
78 the Kuosheng spent fuel pool and to confirm that the existing configuration can provide enough
79 cooling to meet licensing regulations with a maximum water temperature of 60 °C. A unique
80 aspect of their work is that they used CFD in a more advanced way than in other studies to
81 predict local boiling within the pool water, reflecting the strength of the CFD approach.
82 Another use of CFD is to study flow characteristics within fuel assemblies. For example, a
83 study conducted by Chen et al. [13] investigated flow and heat transfer within a rod bundle
84 using a three-dimensional model.

85 Yanagi et al. [14] produced a CFD model for a cooling pond and compared the predicted water
86 temperature with those for the cooling pond at Fukushima Daiichi Nuclear Power Station under
87 loss of cooling conditions. The water surface was modelled using a previously derived heat
88 transfer correlation by the same authors [15]. The CFD model produced by Yanagi et al. [14]
89 was further used to form a baseline for an analytical model "One-Region model" also generated
90 by Yanagi et al. [16, 17]. This One-Region treats the water as one node with a single temperature
91 value without taking into consideration its distribution. After that, they have examined the
92 effect of the distribution of the heat load on the variation of water temperature and it was
93 confirmed that the One-Region model applicable to predict the water temperature in the cooling
94 pond during the loss of cooling scenario.

95 On the other hand, most of the studies adopting the system codes were concerned about
96 investigating accident scenarios and their consequences. Carlos et al. [18] used the TRACE
97 best estimate code to analyse the safety of the Maine Yankee spent fuel pool. Ognerubov et al.
98 [19] investigated scenarios of the loss of water in a spent fuel pool in the Ignalina NPP using
99 various system codes to identify potentially unrealistic parameters while performing the
100 calculations. Groudev et al. [20] used RELAP5 to study the thermal-hydraulic behaviour of
101 spent fuel for a dry out scenario while transferring fuel from the Kozloduy NPP reactor vessel
102 to the cooling pool. Additional studies dealing with fuel ponds can be found elsewhere [5, 21,
103 22].

104 Some investigations concern accident mitigation options using thermal-hydraulic codes. Chen
105 et al. [6] used the GOTHIC code to model a spent fuel pool owned by the Taiwan Power
106 Company to analyse its response to spray mitigation under loss-of-coolant scenarios. Wu et al.
107 [23] conducted an analysis of the loss of cooling accident scenarios for a spent fuel pool at the
108 CPR1000 NPP using the MAAP5 code. In the same study, the authors discussed mitigation
109 measures to recover the pool cooling system using make-up water.

110 The literature cited above shows that the CFD approach is more convenient when it comes to
111 improving the design of cooling ponds, as it offers an in-depth understanding of heat and mass
112 transfer and fluid mixing. On the other hand, thermal-hydraulic system codes such as TRACE
113 are more suitable for analysing safety issues with such ponds and when the system under
114 consideration can be approximated to one-dimensional flow.

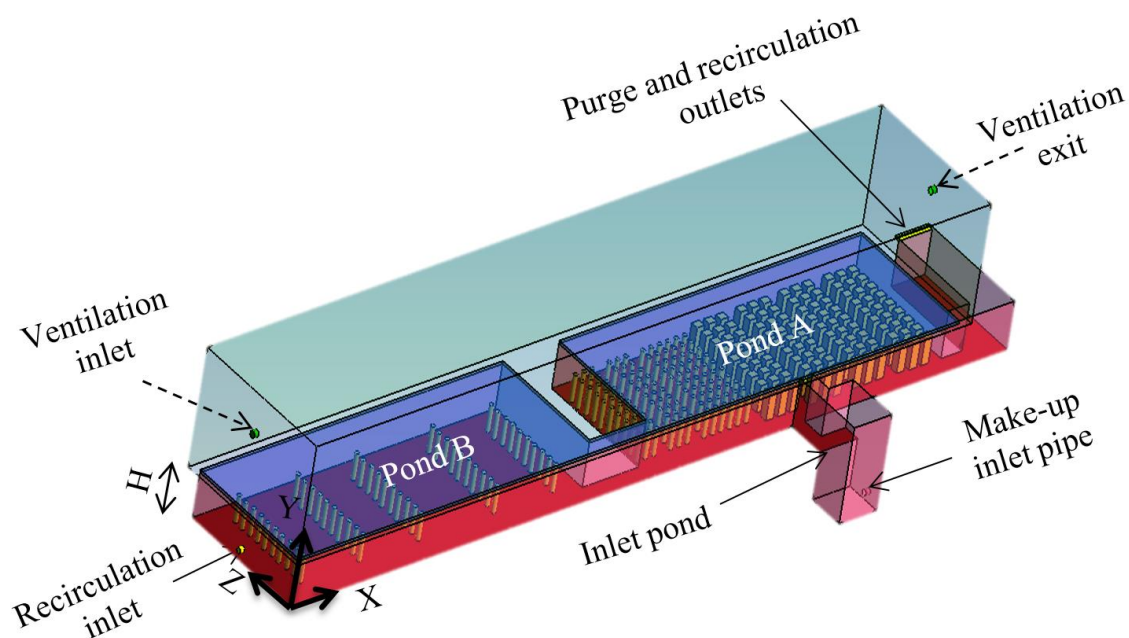
115 In general, most studies focus on investigations of severe accident scenarios and the analysis
116 of their consequences. However, relatively few studies have reported on improving pond
117 design as well as accident mitigation options. Conversely, very limited number of studies have
118 investigated the thermal performance of spent fuel cooling ponds during normal operating
119 conditions, which may represent the first line of defence in accident prevention.

120 It is worth noting that most spent fuel cooling ponds considered in the cited studies are of
121 relatively small size. On the other hand, due to the continuing increase in spent fuel production,
122 some countries are tending to construct centralised cooling ponds to keep up with demand from
123 incoming spent fuel until a more permanent solution is found [24, 25]. To date, centralised,
124 large-scale, ponds have been little discussed in literature, and this may be attributable to the
125 challenges encountered during the modelling and analysis of such systems.

126 In this paper, we explore the suitability of adopting the well-mixed approach in developing a
127 Z-D model for a large-scale cooling pond. The well-mixed approach is widely used in
128 ventilation applications to predict the concentration of specific gases or vapours in a room [26].
129 This model treats the room as a large box, which is perfectly mixed so that the concentration
130 of gas or vapour is uniform.

131 The proposed Z-D model is able to provide a quick answer for “what-if” scenarios, which is
132 necessary at the decision-making stage to aid organisations in more efficient operation of their
133 cooling ponds. Also, the Z-D model will allow, in future work, the thermal performance of the
134 large-scale cooling ponds to be analysed. Also, the outcomes from the proposed model can be
135 coupled with the numerical approach to provide some boundary conditions in the CFD analysis
136 for both macro and micro level model of the pond. For example, the coupling can be achieved
137 via specifying the boundary condition at the free water surface in the CFD model instead of
138 modelling the humid air zone, which involved multiphase models.

139



140

141

Figure 1. Schematic diagram of the large-scale fuel pond.

142

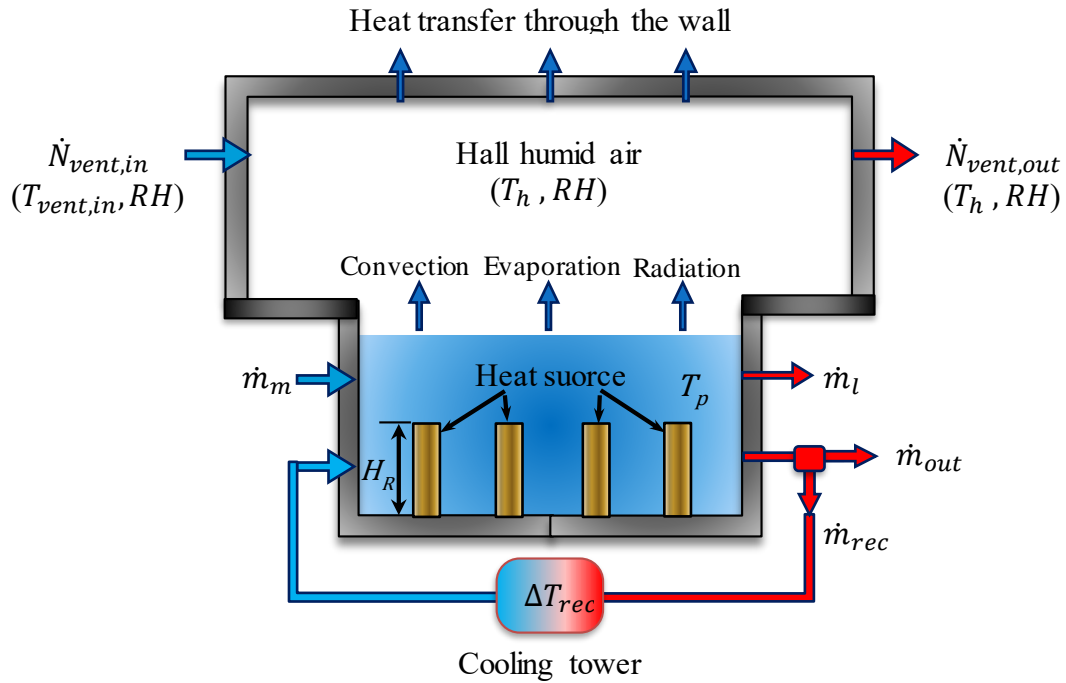
143 **2 Large-Scale Cooling Pond under investigation**

144 Figure 1 shows a schematic diagram of the large-scale cooling ponds in a three-dimensional
145 view. The ponds are characterised by large dimensions of 160m x 25m x 8m and the water
146 surface area is about 3500 m². The whole installation consists of three different ponds. The
147 entire facility includes three different ponds. Pond A and Pond B store the heating sources
148 while the inlet pond supplies make-up. Heat removal takes place via three mechanisms:
149 ventilation, make-up water and water recirculation as illustrated in Figure 2. When the heat is
150 released from the heat sources, the water temperature starts to increase as does the heat transfer
151 from the water surface to the ambient air. The heat transfer from the water surface takes place
152 via three heat transfer modes: evaporation, convection, and radiation. The ventilation system
153 is used to replace the warm air within the building with relatively cooler air. The major heat
154 loss from the water surface is due to the evaporative component; however, this is associated
155 with the loss of pond water, which may lead to a significant drop in the water level in the long
156 term. For this reason, make-up water can be supplied to the pond to prevent the potential risk
157 of uncovering the heat sources. Furthermore, make-up water can be used for purging the pond
158 water as it has been demineralised before reaching the pond. The temperature of the make-up
159 water is mostly determined by the outside temperature.

160 Recirculation can be used on occasions when cooling by ventilation and make-up water is not
161 sufficient to control the pond temperature. Cooling via recirculation is achieved by feeding
162 some of the pond water through a cooling tower which then re-enters the pond a few degrees
163 cooler. However, cooling is not the only function of recirculation. It also helps to reduce
164 unfavourable thermal stress in the pond's concrete walls which may otherwise lead to cracks
165 and the leakage of contaminated water. This is achieved by maintaining the water temperature
166 as uniformly distributed as possible, preventing excessive cracking in the pond walls.

167 Also, due to the long storage time of the heat load under water, a caustic dosing is injected to
168 protect the fuel cladding from any potential corrosion as well as to assist with the removal of
169 colour and turbidity present in the cooling water. In addition, the operational experience
170 showed that such chemical could help to reduce cracks in the concrete walls. In such situation,
171 recirculation of the pond water is required to improve the dispersion of the caustic dosing by
172 recirculating the pond water at various locations across the pond.

173

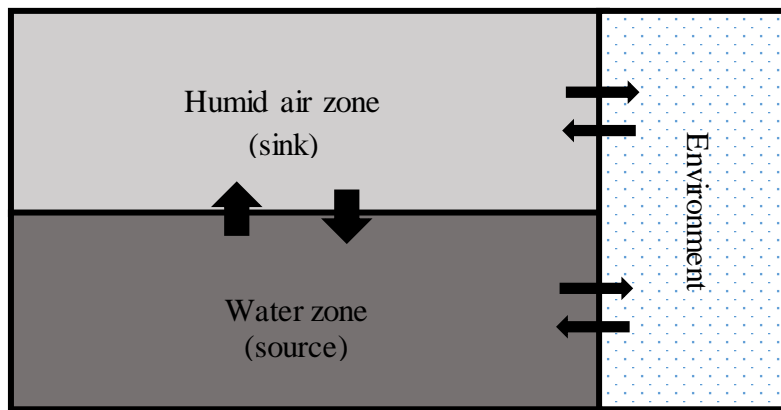


174

175

Figure 2. Description of the processes taking place within the pond installation.

176



177

178

Figure 3. Zones used in the Z-D model.

179

180 3 Z-D Model

181 While developing the Z-D model for the cooling ponds, the whole pond installation is divided
 182 into two nodes: the humid air zone and water zone as shown in Figure 3. These zones can be
 183 described as a source and a sink, where the water zone acts as the source of water vapour and

184 heat energy and humid air zone acts as the sink. Energy and mass transfer with the environment,
185 the third zone, is also integral part of the model

186 The well-mixed approach is adopted in both zones. Since the heat sources are located at the
187 bottom of the pond, the water temperature for the bulk of the pond can be assumed to be
188 uniformly distributed due to buoyancy-induced convection. Similarly, the temperature of the
189 humid air zone can be treated a single value due to the large volume and the flow process of
190 evaporation. Experimental data from the site also support the above assumption.

191 The proposed Z-D model is based on solving conservation of mass and energy equations for
192 the water body and humid air zone above the water surface. The model treats each zone as a
193 single control volume and takes into account heat and mass transfer as well as interaction at
194 the air-water interface. The environment provides some boundary conditions such as
195 temperature and relative humidity to solve the ODEs involved water and humid air zones.

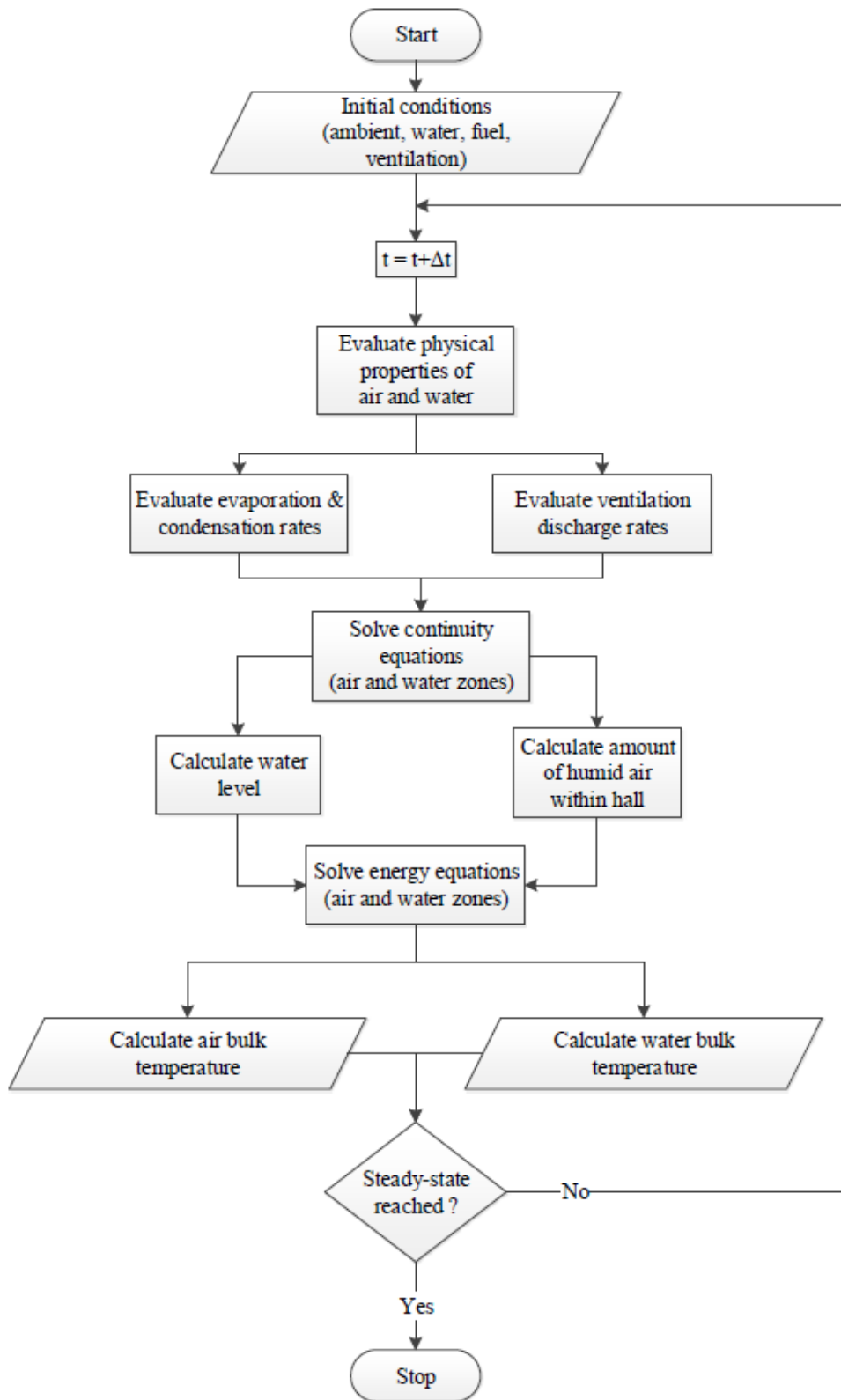
196 The forward time marching approach is adopted to solve a system of differential equations of
197 mass and energy using Euler's forward method as a discretization scheme [27]. This is an
198 explicit method where the solution of the current time step depends on information from the
199 previous step. The general form of Euler's method is shown in Eq. (1). The advantage of this
200 approach is that it does not require significant computing time or power and allows the
201 calculations to be performed using Microsoft Excel spreadsheet

202

$$x^{n+1} = x^n + f(t^n, x^n)\Delta t \quad (1)$$

203

204 A diagrammatic representation of the Z-D model is illustrated in Figure 4. In the beginning,
205 initial values are given to start the solution. The physical properties of air and water are
206 evaluated at each time step. After that, the mass fluxes across the pond structure, evaporation
207 and condensation rates, are estimated along with the ventilation discharge rate. At this point,
208 two mass balance equations are solved in order to calculate the amounts of air and water, which
209 are needed to solve the energy equation in each zone. Finally, air and water temperatures are
210 obtained for this time step. The new temperature will be used to recalculate the physical
211 properties of air and water for the next time step. This is an iterative process that will continue
212 until the steady state is reached.



213

214

Figure 4. Flowchart representation of the Z-D model.

215

216 **3.1 Mass Balance of the Water Zone**

217 The water in the pond is evaluated at each time step, considering any change due to the supply
 218 of make-up water (\dot{m}_m) and loss of water due to evaporation (\dot{m}_{ev}), leakage (\dot{m}_l), and water
 219 outflow (\dot{m}_{out}). Therefore, the mass balance equation for pond water can be written as follows:

220

$$m_p^{n+1} = m_p^n + (\dot{m}_m - \dot{m}_{out} - \dot{m}_{ev} - \dot{m}_l)^n \Delta t \quad (2)$$

221

222 where m_p is the total mass of water within the ponds, Δt is the time step size, and n is the
 223 number of iterations.

224 The following equation describes how the water outflow from the pond is controlled. When
 225 the water loss due to evaporation and leakage is greater than the supplied make-up water, no
 226 water discharge will be permitted. Similarly, in situations when the height of the water level
 227 (H) is lower than its designed value (H_D), no water outflow is allowed until the water level
 228 reaches this value. The following relationship explains how the outflow of water can be
 229 mathematically expressed:

230

$$\dot{m}_{out} = \begin{cases} 0 & \text{if } (\dot{m}_{ev} + \dot{m}_l) \geq \dot{m}_m \\ \dot{m}_m - \dot{m}_{ev} - \dot{m}_l & \text{if } (\dot{m}_{ev} + \dot{m}_l) < \dot{m}_m \\ 0 & \text{if } H \leq H_D \\ \left[\frac{\rho_w A_p (H - H_D)}{\Delta t} \right] + (\dot{m}_m - \dot{m}_{ev} - \dot{m}_l) & \text{if } H > H_D \end{cases} \quad (3)$$

231

232 where ρ_w is the water density and A_p is the water surface area of the pond. The evaporation
 233 rate before the pond water starts to boil can be estimated using Stefan's law [28]. The following
 234 equations show how the evaporation rate can be estimated before boiling and in the case of
 235 boiling.

236

$$\dot{m}_{ev} = \begin{cases} h_{ev} \log \left(\frac{P_t - P_{v,s}}{P_t - P_{v,\infty}} \right) A_p & \text{if } T_p < T_{sat} \\ \dot{Q}_d / h_{fg} & \text{if } T_p \geq T_{sat} \end{cases} \quad (4)$$

237

238 where, $P_{v,s}$ is the saturated vapour pressure at surface temperature, and $P_{v,\infty}$ is the vapour
 239 pressure at the hall temperature, P_t is the total pressure of humid air inside the hall, h_{fg} is the
 240 latent heat of vaporization for water, \dot{Q}_d is the released heat from the heating elements, T_p is
 241 the pond water temperature, T_{sat} is water saturation temperature and h_{ev} is the evaporative
 242 mass transfer coefficient which can be calculated using the analogy between heat and mass
 243 transfer using Sherwood–Rayleigh power law, $Sh - Ra$, as shown below [28]:

244

$$Sh = \begin{cases} 0.54 Ra_{ev}^{1/4} & \text{if } 10^4 \leq Ra_{ev} \leq 10^7 \\ 0.15 Ra_{ev}^{1/3} & \text{if } 10^7 \leq Ra_{ev} \leq 10^{11} \end{cases} \quad (5)$$

245

246 where Ra_{ev} is the Rayleigh number for mass transfer by evaporation. The definition of Ra_{ev}
 247 can be expressed as shown below:

248

$$Ra_{ev} = Gr \cdot Sc = \left(\frac{g \Delta \rho L^3}{\rho_{av} \nu^2} \right) \cdot Sc \quad (6)$$

249

250 here Gr is the Grashof number and L is the characteristic length, which is considered to be the
 251 area of the water surface over its perimeter.

252

253 3.2 Pond Water Elevation

254 The pond water level is calculated by knowing the water volume and the surface area of the
 255 pond water. When the water level drops to a value less than the rack height (H_R) shown in
 256 Figure 2, the surface area of the water will be limited to the surface area of water between the

257 rack assemblies (A_R). The water level at every time step is updated according to the mass of
 258 water available in the pond, as shown in the following equation:

259

$$H = \begin{cases} \left[\left(\frac{m_p}{\rho_w} - A_R H_R \right) / A_p \right] + H_R & \text{if } H \geq H_R \\ \left(\frac{m_p}{\rho_w} \right) / A_R & \text{if } H < H_R \end{cases} \quad (7)$$

260

261 3.3 Mass Balance of the Humid Air Zone

262 Humid air is considered as a mixture of dry air and water vapour. Both dry air and water vapour
 263 at low partial pressure can be treated as a perfect gas. When dealing with humid air, it is more
 264 convenient that the mass of the moist air to be expressed in mole basis for the dry air and vapour
 265 separately.

266 In order to evaluate the amount of dry air (N_a) and vapour (N_v) inside the pond hall, the mass
 267 balance equation across the hall is applied as shown in Equations (8) and (9). This mass balance
 268 takes into account the ventilation inlet ($\dot{N}_{vent,in}$) and discharge ($\dot{N}_{vent,out}$) flow rates as well
 269 as evaporation and condensation (\dot{m}_{con}) rates.

270

$$N_a^{n+1} = N_a^n + (y_{vent,in}^a \dot{N}_{vent,in} - y_h^a \dot{N}_{vent,out})^n \Delta t \quad (8)$$

271

$$N_v^{n+1} = N_v^n + \left(\dot{N}_{vent,in} - y_h^v \dot{N}_{vent,out} + \frac{\dot{m}_{ev}}{M_v} - \frac{\dot{m}_{con}}{M_v} \right)^n \Delta t \quad (9)$$

272

273 where $y_{vent,in}^a$ is the molar fractions of dry air of the incoming ventilation air and y_h^a and y_h^v
 274 are the molar fractions of dry air and water vapour respectively, which can be found from:

275

$$y_h^a = \frac{N_a}{N_h} \quad (10)$$

276

$$y_h^v = \frac{N_v}{N_h} \quad (11)$$

277

$$N_h = N_a + N_v \quad (12)$$

278

279 Here N_h is the total molar mass of the humid air inside the pond hall. The flow rate of the
280 ventilation inlet is an initial input condition, where the differential pressures drive the
281 ventilation discharge and can be computed from:

282

$$\dot{N}_{vent,out} = \rho_\infty M_v A_{duct} \sqrt{\frac{2(P_t - P_{atm})}{\rho_\infty}} \quad (13)$$

283

284 where ρ_∞ is the density of the humid air inside the pond hall, M_v is the molecular weight of
285 water vapour, A_{duct} is the cross-sectional area of the ventilation discharge duct, P_{atm} is the
286 outside atmospheric pressure P_t is the total pressure of humid air inside the pond hall and can
287 be evaluated as follow:

288

$$P_t = \left(\frac{T_h R_o}{V_h} \right) N_h \quad (14)$$

289

290 The estimation of the condensation rate is similar to the calculation of the evaporation rate:

291

$$\dot{m}_{con} = h_{con} (\rho_{v,\infty} - \rho_{v,wall}) A_h \quad (15)$$

292

293 where, $\rho_{v,wall}$ is the saturated vapour density at wall temperature, A_h is surface area of the
294 inner walls of the pond hall and h_{con} is the condensation mass transfer coefficient which can
295 be calculated from:

296

$$Sh = 0.10 Ra^{1/3} \quad (16)$$

297

298 To examine the coefficient 0.10 in Eq. (16), we have run several calculations considering
299 different values for this coefficient ranging from 0.05 to 0.2. It was found that the maximum
300 effect of this coefficient on the final result for the water temperature is relatively low, less than
301 1.5%.

302 **3.4 Energy Balance of the Water Zone**

303 The energy contained in the water body is integrated over time taking into account the heat
304 realised from the heat sources, the heat flux from the water surface and the energy associated
305 with the water inlets and outlets:

306

$$T_p^{n+1} = T_p^n + \left(\dot{Q}_d + \dot{m}_m C_w T_m - \dot{m}_{out} C_w T_p - \dot{m}_{ev} C_w T_p - \dot{m}_{rec} C_w \Delta T_{rec} - \dot{Q}_s \right)^n \frac{\Delta t}{m_p C_w} \quad (17)$$

307

308 where C_w is the specific heat of water, T_m is the temperature of the make-up water, \dot{m}_{rec} is the
309 recirculation flow rate, ΔT_{rec} is the temperature drop in the cooling tower which is controlled
310 by the wet bulb temperature of the outdoor air (T_{wb}) and the cooling tower efficiency and can
311 be expressed as:

312

$$\zeta = \frac{\Delta T_{rec}}{T_p - T_{wb}} \quad (18)$$

313

314 and \dot{Q}_s is the total heat transfer at the air-water interface which can be estimated as shown
315 below:

316

$$\dot{Q}_s = \dot{Q}_{ev} + \dot{Q}_r + \dot{Q}_c \quad (19)$$

317

318 where \dot{Q}_{ev} is the evaporative heat transfer, \dot{Q}_r is the radiative heat transfer, and \dot{Q}_c is the
 319 convective heat transfer. These three heat transfer modes can be evaluated from the following
 320 expressions:

321

$$\dot{Q}_{ev} = \dot{m}_{ev} h_{fg} \quad (20)$$

322

$$\dot{Q}_r = A_p \varepsilon \sigma (T_p^4 - T_{wall}^4) \quad (21)$$

323

$$\dot{Q}_c = A_p h_c (T_p - T_h) \quad (22)$$

324

325 Here ε is emissivity, σ is the Stefan Boltzmann constant, T_{wall} is the wall inner surface
 326 temperature of the hall, h_c is the convection heat transfer coefficient at the water surface which
 327 may be evaluated by using the Nusselt–Rayleigh power law, $Nu - Ra$, as shown below:

328

$$Nu = \begin{cases} 0.54 Ra^{1/4} & \text{if } 10^4 \leq Ra \leq 10^7 \\ 0.15 Ra^{1/3} & \text{if } 10^7 \leq Ra \leq 10^{11} \end{cases} \quad (23)$$

329

330 3.5 Energy Balance of the Humid Air Zone

331 The heat loss from the water surface is gained by the ventilated air, which results in an increase
 332 in air temperature. To calculate the air temperature inside the pond hall, the energy balance is
 333 performed across the hall as shown below:

334

$$T_h^{n+1} = T_h^n + \left[\dot{m}_{ev} h_v (T_p) + \dot{Q}_c + \dot{Q}_r - \dot{Q}_{wall} - \dot{m}_{con} h_{fg} + \dot{Q}_{vent,in} - \dot{Q}_{vent,out} \right]^n \frac{\Delta t}{[N_a M_a C_{p,a} + N_v M_v C_{p,v}]} \quad (24)$$

335

336 where $h_v(T)$ is the specific enthalpy of water vapour at a given temperature and can be
337 calculated using the shown below [29]. However, this relationship is valid only for low values
338 of pressure.

339

$$h_v(T) = 2500 + 1.82 (T - 273) \quad (25)$$

340

341 In order to obtain the heat energy associated with the incoming ventilated humid air ($\dot{Q}_{vent,in}$)
342 and the discharged humid air by ventilation ($\dot{Q}_{vent,out}$), the following relationships are used:

343

$$\dot{Q}_{vent,in} = y_{vent,in}^a \dot{N}_{vent,in} C_{p,a} T_{vent,in} + y_{vent,in}^v \dot{N}_{vent,in} h_v(T_{vent,in}) \quad (26)$$

344

$$\dot{Q}_{vent,out} = y_h^a \dot{N}_{vent,out} C_{p,a} T_h + y_h^v \dot{N}_{vent,out} h_v(T_h) \quad (27)$$

345

346 Here, $y_{vent,in}^a$ and $y_{vent,in}^v$ are the molar fractions of the ventilation inlet dry air and vapour
347 respectively, $C_{p,a}$ is the specific heat of the dry air, and $T_{vent,in}$ is the ventilation inlet
348 temperature which is assumed to be the same as the outside temperature. The heat transfer
349 through the walls of the pond hall (\dot{Q}_{wall}) is computed according to:

350

$$\dot{Q}_{wall} = h_{in} (T_h - T_{wall}) A_h \quad (28)$$

351

352 In order to determine T_{wall} , an energy balance is performed across the walls of the pond hall
353 where the wall thickness (x) is divided to uniform increments of dx . The energy equations for
354 the interior and surface layers can be written as follow:

355

$$T_i^{n+1} = T_i^n + \frac{k}{dx C_{wall} \rho_{wall}} \left(\frac{T_{i-1} - T_i}{dx} - \frac{T_i - T_{i+1}}{dx} \right)^n \Delta t \quad (29)$$

356

$$T_i^{n+1} = T_i^n + \frac{k}{dx C_{wall} \rho_{wall}} \left(\frac{T_{wall} - T_i}{dx/2} - \frac{T_i - T_{i+1}}{dx} \right)^n \Delta t \quad (30)$$

357

358 where i is the index of the wall layers, C_{wall} is the specific heat of the walls material, ρ_{wall} is
 359 the density of the walls material, and k is the thermal conductivity of the walls material. The
 360 inner and outer surface temperatures can be calculated considering the heat balance across this
 361 surface as shown below, respectively:

362

$$\dot{Q}_r + (T_h - T_{wall}) A_h h_{in} = \frac{T_{wall} - T_i}{dx/2} A_h k \quad (31)$$

363

$$(T_{out} - T_{env}) A_h h_{out} = \frac{T_i - T_{out}}{dx/2} A_h k \quad (32)$$

364

365 where T_{env} is the outside environment temperature h_{in} is the convective heat transfer
 366 coefficient for the inner surface of the pond hall and h_{out} is the outer surface heat transfer
 367 coefficient and was considered to be constant (4 W/m² K). Finally, under the normal
 368 operational conditions, the solution is considered to be converged when the relative difference
 369 between the current iteration and the previous iteration is less than 0.01%. The convergence
 370 criterion is expressed as shown below:

371

$$\text{Convergence criterion} = \frac{|T_p^{n+1} - T_p^n|}{T_p^n} \times 100 \quad (33)$$

372

373 However, this convergence criterion cannot be applied when the pond is suffering from loss of
 374 cooling. In this case, the temperature of the pond water will continue to increase until the

375 saturation is reached. During this time, the water level may drop until the pond dries out unless
 376 sufficient make-up water is provided to compensate for the evaporated water.

377

378 The heat loss from the pond water to the concrete wall is not considered in this study as it
 379 makes only a tiny contribution to the total heat loss from the pond's structure. This is because
 380 the ponds are surrounded by a very thick concrete layer at the sides and floor.

381 As mentioned before, the calculations were performed using the explicit Euler's method, which
 382 is known to be conditionally stable, hence, a stability analysis is required [30]. Investigation of
 383 the numerical behaviour of the model shows that the stability of the model is more dominated
 384 by the stability of the differential equations rather than the used method. The highest instability
 385 was observed in the mass balance equation for the humid air zone. This is due to the pressure
 386 fluctuation, which is mostly controlled by the ventilation discharge. Therefore, a stability
 387 analysis is conducted on the mass balance equation for the humid air zone. However, to perform
 388 such analysis, the nonlinear equations have to be linearized. The linearization of the ODE for
 389 the mass balance of the humid air zone was achieved using Taylor series. Then, a systematic
 390 stability analysis was accomplished as follows:

- 391 • Construct the finite difference equation (FDE) for the model ODE, $\dot{y} + \phi y = 0$
- 392 • Determine the amplification factor, G , of the FDE.
- 393 • Determine the conditions to ensure that $|G| < 1$.

394 By applying the above-mentioned practice, an estimation of the limit of the stable time step
 395 can be expressed as:

$$\Delta t < \frac{2}{\theta} \tag{34}$$

396

397 where θ is equivalent to:

398

$$\theta = \frac{A_{duct} R_o T_h}{2V_h} \sqrt{\frac{2\rho_\infty}{\left(\frac{T_h R_o}{V_h}\right) N_h^n - P_{atm}}} \tag{35}$$

399

400 Note that θ changes as N_h^n changes. Thus, the stable step size changes as the solution advances.
401 However, keeping the time step within the criterion shown in Eq. (34) not only ensures
402 stability, but it also ensures that the results are not very sensitive to the time step. According to
403 this criterion, the used time step in all the cases presented in this study is 5 sec.

404 **4 Z-D Model Validation**

405 The Z-D thermal model of the cooling pond is validated against available data for two different
406 cooling ponds as shown below:

- 407 1. Maine Yankee spent fuel pool, Wiscasset, USA [18]
- 408 2. The large-scale cooling pond

409 **4.1 Validation with Maine Yankee Pool Data**

410 The Maine Yankee spent fuel pool is a relatively small cooling pond located at the reactor site,
411 with dimensions of 12.6 m long, 11.3 m wide and 11.1 m deep. Carlos et al. [18] used TRACE
412 best estimate code to analyse the response of the cooling pond in different scenarios. During
413 their calculations, no heat loss was considered at the free water surface except when the water
414 has reached its saturation temperature (100 °C) with the initiation of boiling. However, this
415 assumption does not have a significant effect on the results, as the proportion of heat loss from
416 the water surface before boiling is not significant compared to the heat loss by the supplied
417 water. This is owing to the small surface area at the air-water interface.

418 The Z-D model is used to perform calculations on the Maine Yankee spent fuel pool, Wiscasset,
419 USA [18] and the results obtained are compared against the published data for this pool. These
420 calculations are developed for three cases: (a) steady-state, (b) licensing, and (c) accident
421 scenarios.

422 In the paper reported by Carlos et al. [18], the temperature data were available for the steady-
423 state case in the form of actual temperature measurements collected from the Maine Yankee
424 spent fuel pool. For the licensing case, the temperature data were calculated by GFLOW
425 software [31], while the TRACE best estimate code was used for the pool temperature under
426 the accident scenarios.

427 *(a) - (b) Steady-state and Licensing Cases*

428 The input parameters used in the calculations of the steady-state and licensing cases are
 429 summarised in Table 1. In the same table, the outcomes from the validation exercise our Z-D
 430 model are presented. The heat load in the licensing case corresponds to the maximum expected
 431 heat generation from the fuel elements.

432 The results predicted by the Z-D model are in good agreement with the available data for the
 433 Maine Yankee spent fuel pool as can be seen in Table 1. However, the Z-D model
 434 underestimates the pond water temperature by 3 % and 2.6 % for steady-state and licensing
 435 cases respectively. When all of the heat transfer modes from the water surface are deactivated
 436 in the Z-D model calculations, except for boiling, the underestimation errors of the water
 437 temperature decreased to 1.9 % and 0.9 % for the steady-state and licensing cases respectively.
 438 This implies that the heat loss from the water surface before boiling is relatively less significant,
 439 as mentioned before.

440

441 Table 1. Input data and comparison between values predicted by the Z-D model and data for
 442 the Maine Yankee pool [18].

Parameters / Case		Steady State Case	Licensing Case
Heat load (MW)		3.3	6.4
Make-up water flow rate (kg/s)		98	97.6
Make-up water temperature (°C)		26.1	51.7
Water bulk temperature (°C)	Maine Yankee pool [18]	36.7 (measured)	68 (GFLOW)
	Present Z-D model	35.6	66.2
	errors	- 3 %	- 2.6 %

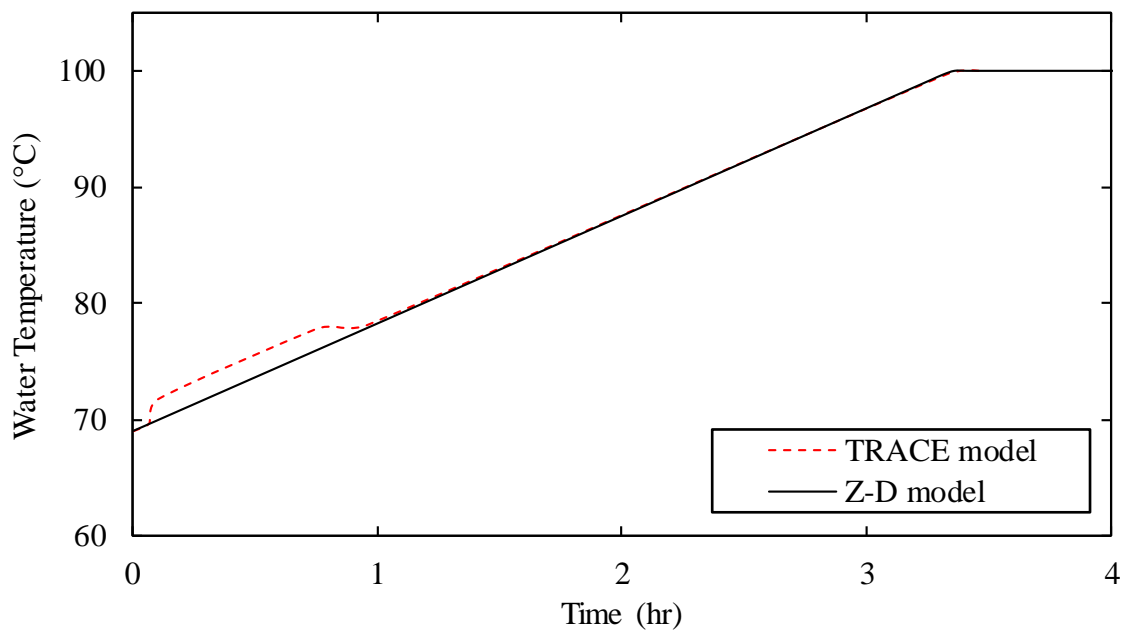
443

444 *(c) Accident Case*

445 The outcomes from the licensing case were used as the input data for the accident scenario
 446 except for the initial water level which is considered to have a value of 4.56 m as measured
 447 from the bottom of the pond. In the TRACE simulation for the accident case, it was assumed
 448 that the pumps which supply the pond with the cooling and make-up water, have stopped
 449 functioning and the only heat loss mechanism available is the heat loss to the surroundings by

450 means of boiling. Therefore, in the Z-D model calculations, the heat transfer modes from the
451 water surface were deactivated and the only heat transfer permitted is due to boiling.

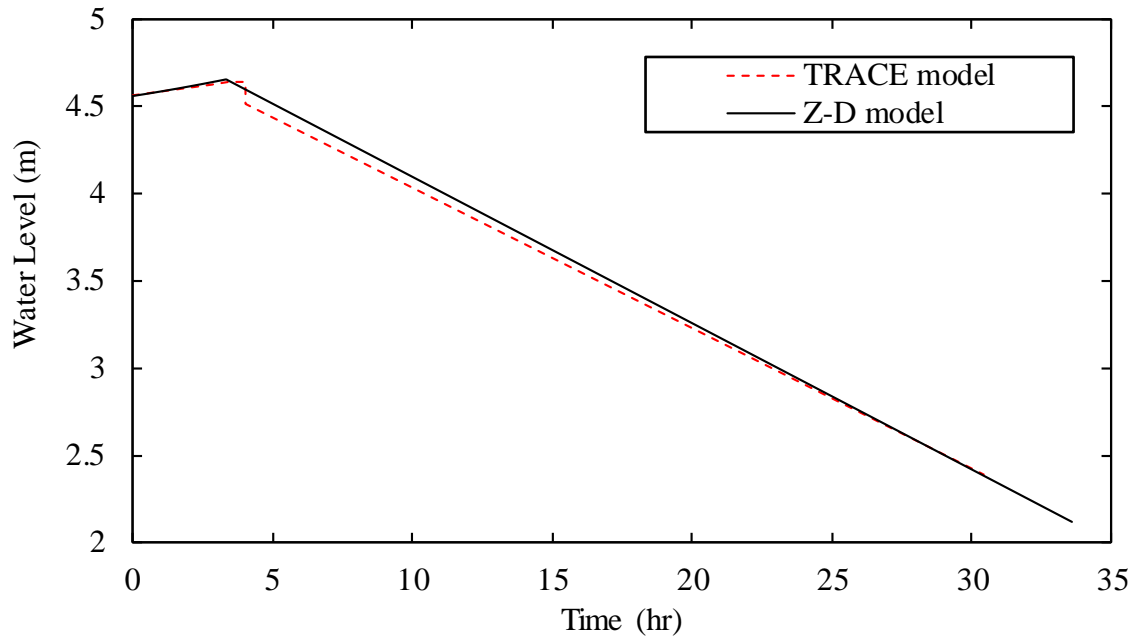
452 Figures 5 and 6 show comparisons between the results predicted by the Z-D model and the
453 TRACE data for the accident scenario in terms of water temperature and drop of pond water
454 level respectively. In Figure 5, for up to one hour the same linear trend is observed, but a clear
455 shift of 1.8 °C is recorded, the reason for which is not obvious from the original paper [18].
456 Figure 6 shows a sudden drop in water level over a very short time (something similar to
457 purging), but the reason for such behaviour was also not explained. These behaviours may be
458 due to assumptions made which are unknown to us. In general, good agreement can be observed
459 between the Z-D model and the TRACE best estimate code.



460

461 Figure 5. Comparison of water temperature for the accident case that obtained by the proposed
462 Z-D model and Maine Yankee pool [18].

463



464

465 Figure 6. Comparison of water level for the accident case that obtained by the proposed Z-D
 466 model and Maine Yankee pool [18].

467 **4.2 Validation with Large-Scale Cooling Pond Data**

468 The validation exercise is further extended to consider a large-scale cooling pond to examine
 469 the effect of pond size on the Z-D model’s prediction. The total heat realised from the heat
 470 sources is about 340 kW.

471 The validation is performed for three different operational configurations and the input
 472 parameters used during these calculations are summarised in

473

474

475

476 Table 2. Comparisons between the measured data and the results predicted by the Z-D model
 477 are presented in tabular form as shown in Table 3. It can be seen from the comparisons that the
 478 Z-D model has predicted the water temperature as well as the hall air temperature within a good
 479 level of accuracy. However, the Z-D model has slightly overestimated the water temperature.
 480 The maximum observed error in the predictions of water temperature is 3.56 %, where the
 481 maximum recorded error in the hall air temperature is - 4.55 %.

482

483

484

485

486 Table 2. Input parameters used in validation with the large-scale cooling pond data.

Parameters	Case 1	Case 2	Case 3
Initial water level (m)	8	8	8
Water surface area (m ²)	3,500	3,500	3,500
Water zone volume (m ³)	21,900	21,900	21,900
Humid air zone volume (m ³)	129,600	129,600	129,600
Heat transfer area of humid air zone (m ²)	15,120	15,120	15,120
Heat load (kW)	340	340	340
Outside environment temperature (°C)	11	14	19
Recirculation flow rate (kg/s)	4.57	4.63	4.05
Temperature drop in cooling tower (°C)	0	0	3
Make-up rate (kg/s)	3.47	3.62	3.84
Make-up temperature (°C)	10	14	20
Ventilation inlet rate (m ³ /s)	12	12	12

487

488 Table 3. Comparison between measured and predicted results for the large-scale cooling
489 ponds data.

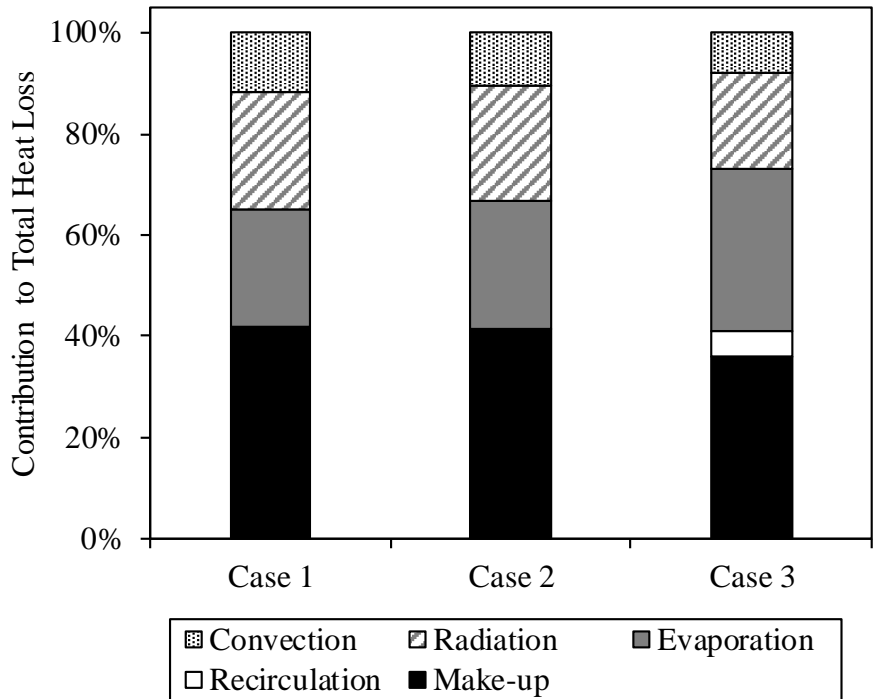
	Water Temperature (°C)			Hall Air Temperature (°C)		
	Measured	Predicted	Error (%)	Measured	Predicted	Error (%)
Case 1	20.6	21.3	3.39 %	18.2	17.5	- 3.85 %
Case 2	23.2	23.9	3.01 %	19.8	18.9	- 4.55 %
Case 3	25.3	26.2	3.56 %	21.7	21.1	-2.76 %

490

491 The percentage contribution of each heat removal mode to the total heat loss is shown in Figure
492 7 for the three validation cases. These contributions are evaluated when the steady state is
493 reached. From the results shown in this figure, it is obvious that the heat loss from the water
494 surface is significant as it represents about 50% of the total heat loss from the ponds. However,

495 under different configurations, these ratios can vary significantly. For an instant, when the
 496 make-up water or recirculation flow rates are high, this will lead to much higher contributions
 497 of these heat removal modes over the surface heat loss.

498



499

500 Figure 7. Contribution percentage of different heat removal modes for validation case 1, case
 501 2, and case 3.

502 **5 Analysis of Pond Behaviour**

503 After confirming the reliability of the Z-D model, it was used to study the thermal behaviour
 504 of the large-scale cooling pond, and in addition, to assess the suitability of using particular
 505 assumptions in certain cases. From the point of view safety and economics, it is essential to
 506 analyse the performance of the pond under normal operating conditions as well as accident
 507 scenarios.

508 **5.1 Normal Operating Conditions**

509 The calculations in this section are performed considering that the pond is loaded with the
 510 maximum possible heat load and all of the cooling systems are in place and under control. The
 511 maximum heat load is 11 MW, which corresponds to the maximum expected amount of heat
 512 sources to be stored and is assumed to be uniformly distributed throughout the pond. The input
 513 parameters used in this calculation are listed in Table 4.

514

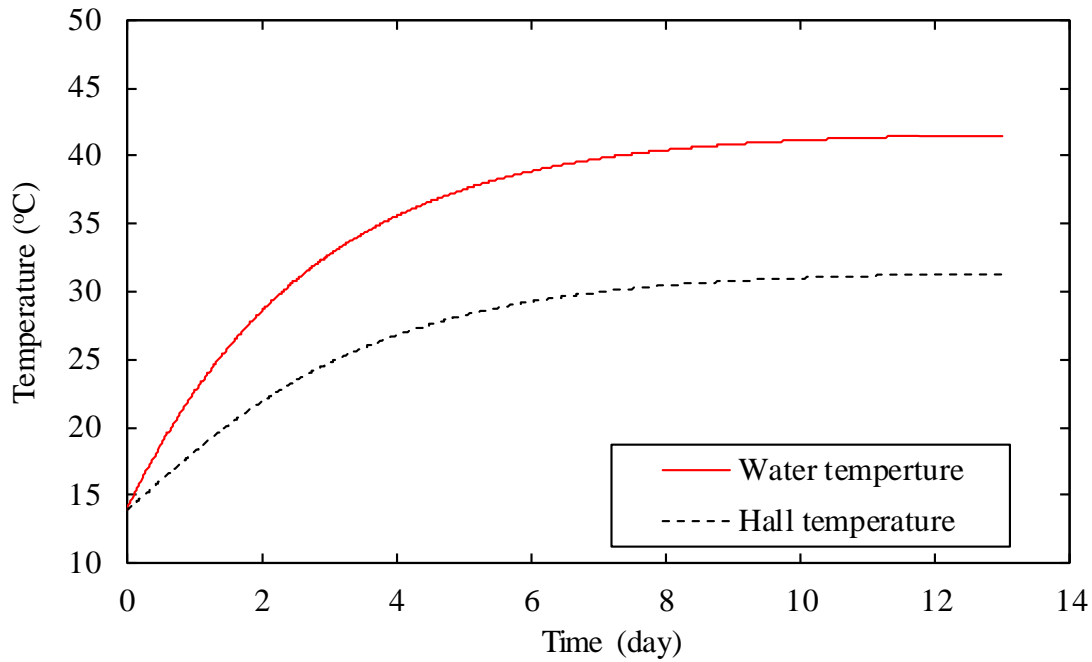
515

Table 4. Configurations used in the case of normal operating conditions.

Parameters	
Initial water level (m)	8
Water surface area (m ²)	3500
Water zone volume (m ³)	21900
Humid air zone volume (m ³)	129600
Heat transfer area of humid air zone (m ²)	15120
Heat load (MW)	11
Outside environment temperature (°C)	14
Recirculation flow rate (kg/s)	115.74
Cooling tower efficiency (%)	60
Make-up rate (kg/s)	13.9
Make-up temperature (°C)	14
Ventilation inlet rate (m ³ /s)	12

516

517 The results for the normal operations case are presented in Figure 8 in terms of water and hall
518 temperatures. As shown in this figure, at the beginning of the calculations the water and air
519 temperatures have the same value of 14 °C. As time progresses, both water and air temperatures
520 increase until the steady state is reached at values of 41.5 °C for the water and about 31.3 °C
521 for the hall air.



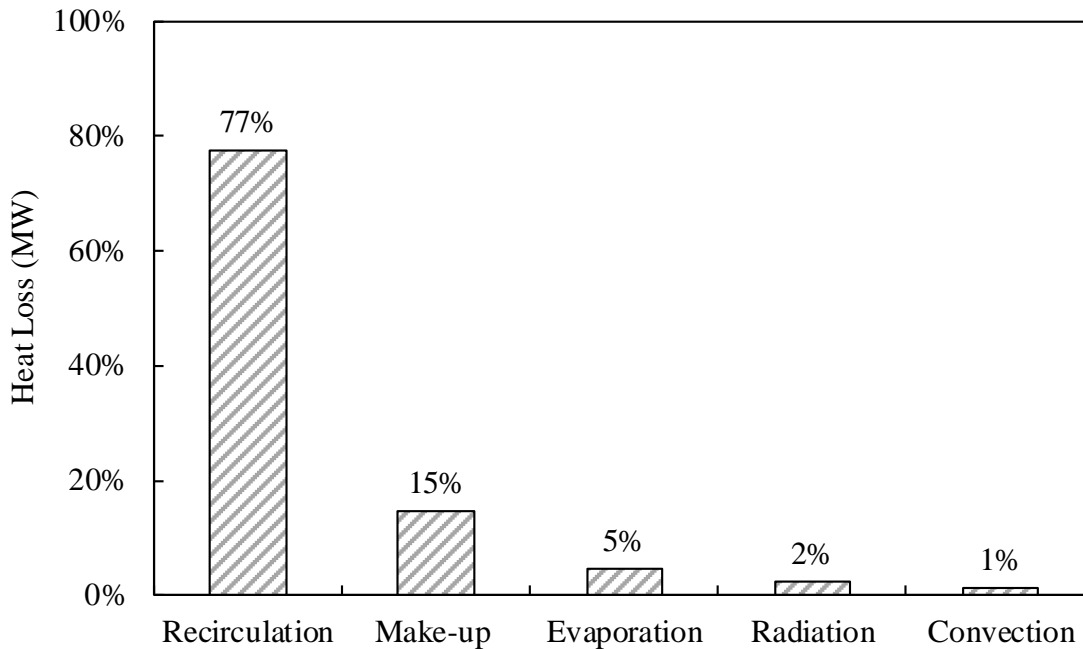
522

523 Figure 8. Water and air temperatures under normal operating conditions for the large-scale
 524 cooling pond at a heat load of 11 MW.

525

526 The generated heat is removed via different modes as shown in Figure 9. Furthermore, this
 527 figure illustrates the contribution of the heat removal component to the total heat removed from
 528 the water body. The generated heat being removed by the recirculation is dominated the cooling
 529 process with a percentage of 75 % of the total heat loss. It appears that the heat loss from the
 530 water surface represents a relatively small proportion (8%) of the total heat loss, but it cannot
 531 be ignored. However, the scenario can be different for lower heat loads as in the cases presented
 532 in the validation section for the large-scale cooling ponds as shown in Figure 7.

533



534

535 Figure 9. The contribution of different heat removal modes under normal operating conditions
 536 for the large-scale cooling pond.

537

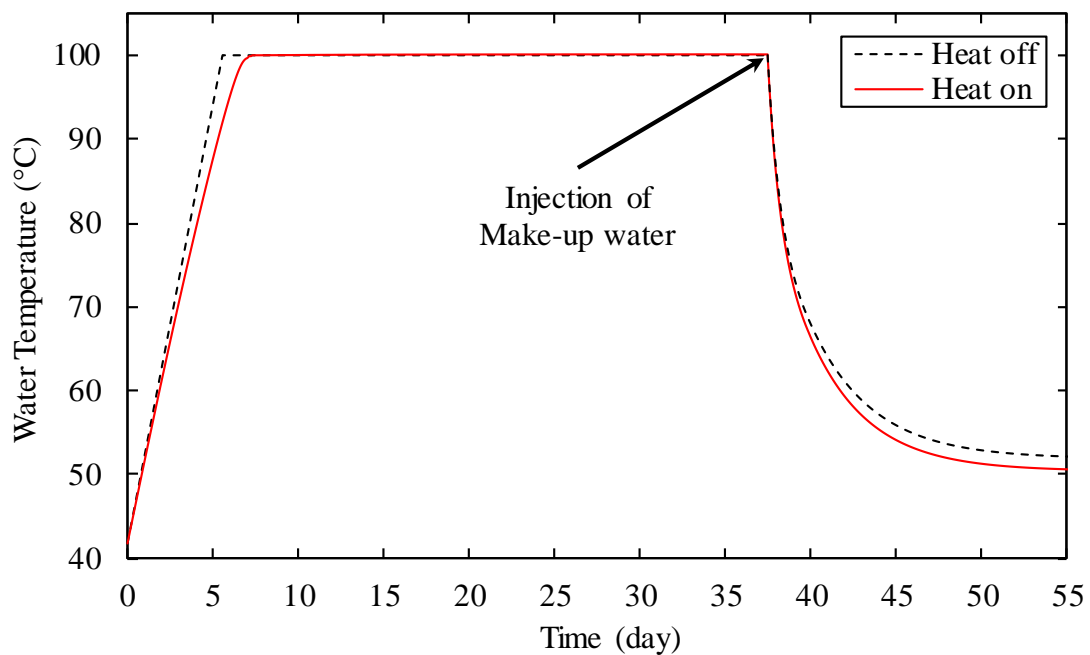
538 **5.2 Loss of Cooling Scenario**

539 In this section, we assume that a power blackout and total loss of the cooling systems occurs
 540 with no accident mitigation measures in place. The calculations are conducted for the large-
 541 scale cooling pond taking the outcomes from the previous case of normal operating conditions
 542 as initial values. Moreover, the calculations are performed for two different conditions at the
 543 water surface. The first condition ignores the heat loss from the water surface except for the
 544 boiling heat transfer, which is represented in the graphs by “Heat off”. The second condition
 545 takes into account all the heat transfer modes at the water surface, which is represented in the
 546 graphs by “Heat on”.

547 As can be seen from Figures 10 and 11 that at the “Heat off” condition, the water temperature
 548 reaches boiling after 5.6 days. Meanwhile, the water level reaches its highest value due to a
 549 decrease in water density and then starts to drop until the fuel assemblies begin to be uncovered
 550 at approximately day 37. At this point, make-up water is injected to recover the pond water
 551 temperature and level. To achieve this, 2.5 days is required to recover the water level and 18
 552 days for the water temperature to drop to about 50.7 °C.

553 For the “Heat on” condition, the estimation of the time required for the fuel assembly to start
554 to be uncovered is the same as in the “Heat on” case. On the other hand, water reaches its
555 saturation temperature 2 days earlier than the predicted time in the “Heat on” case. However,
556 these differences, in the presented case, are still within a good level and provide a conservative
557 treatment for the accident scenario. For different conditions, the assumption that the heat loss
558 from the water surface can be neglected may not be appropriate. For example, Figure 12 shows
559 the effect of heat load on the validity of this assumption for different heat loads.

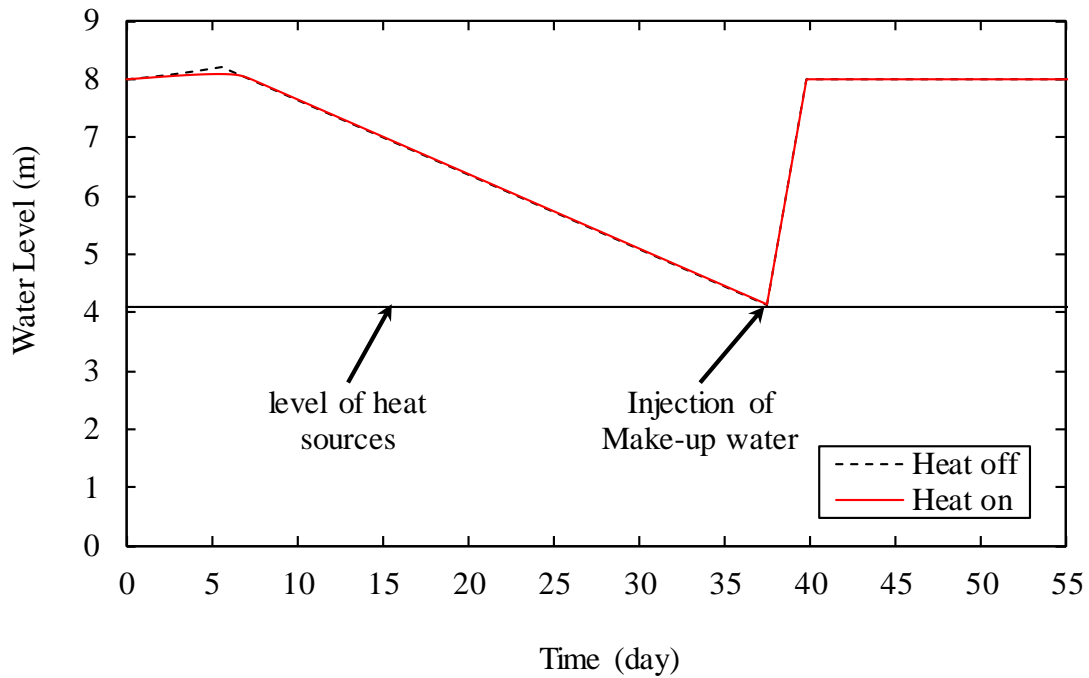
560



561

562 Figure 10. Water temperature during the loss of cooling scenario and after injection of make-
563 up water for the large-scale cooling pond.

564

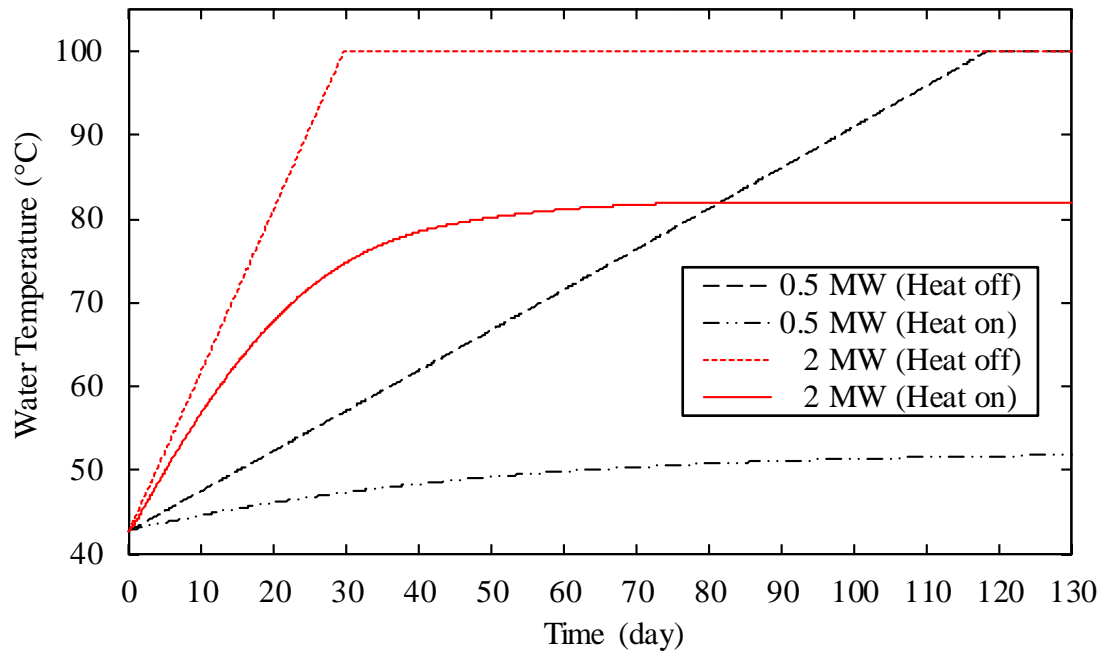


565

566 Figure 11. Water level during the loss of cooling scenario and after injection of make-up water
 567 for the large-scale cooling pond.

568 In Figure 12, for the “Heat off” situation, the sensible heating is faster for the high heat load
 569 and once the temperature reaches the boiling point, for both heat loads, the curves become
 570 parallel to X-axis. It can also be seen that adopting such “Heat off” assumption can significantly
 571 overpredicts the water temperature especially for low heat load values. In Figure 12, the
 572 difference between the predictions of water temperature using both assumptions is around 48%
 573 for a heat load of 0.5 MW, whereas only 18% is observed for the heat load of 2 MW. This
 574 implies that the over-prediction is higher for the low heat load. This is due, as discussed before,
 575 to the large exposed area of the water surface to the ambient air, which increases the surface
 576 heat loss. Hence, such an assumption should be carefully considered while performing the
 577 analysis of accident scenarios for large-scale cooling ponds.

578



579

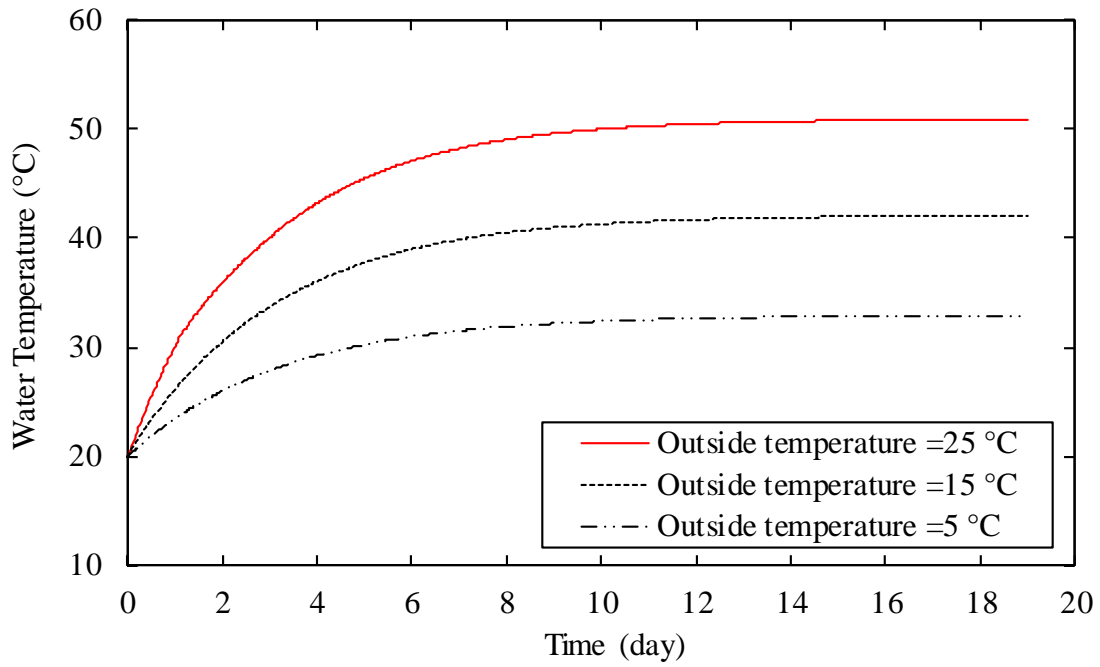
580 Figure 12. Water temperature under different heat loads for the large-scale cooling pond.

581

582 5.3 Impact of Weather Conditions

583 The outside weather conditions are represented in the Z-D model in terms of outside air
 584 temperature and relative humidity. Changes in these conditions may have an effect on the
 585 cooling performance of the spent pond. To examine the potential effects, we have conducted a
 586 sensitivity study by varying the outside air temperature and relative humidity. As can be seen
 587 in Figure 13, the outside air temperature has a significant effect on the water temperature.
 588 Increasing the outside air temperature by about 10 °C results in an increase in the water
 589 temperature by approximately 9 °C. This is because of the make-up water and ventilation air
 590 temperatures are mostly determined by the outside temperature. Also, the temperature drop in
 591 the cooling tower, as shown in Figure 2, is affected by the conditions outside.

592 On the other hand, the relative humidity of the outside air does not have a considerable effect,
 593 as shown in Figure 14. This may be because of the air change per hour (ACH) for the pond hall
 594 is very low for this type of applications, at about 0.333 per hr. Meanwhile, the amount of water
 595 vapour emerging from the water surface due to evaporation is high enough to rapidly increase
 596 the relative humidity of the moist air within the pond hall.

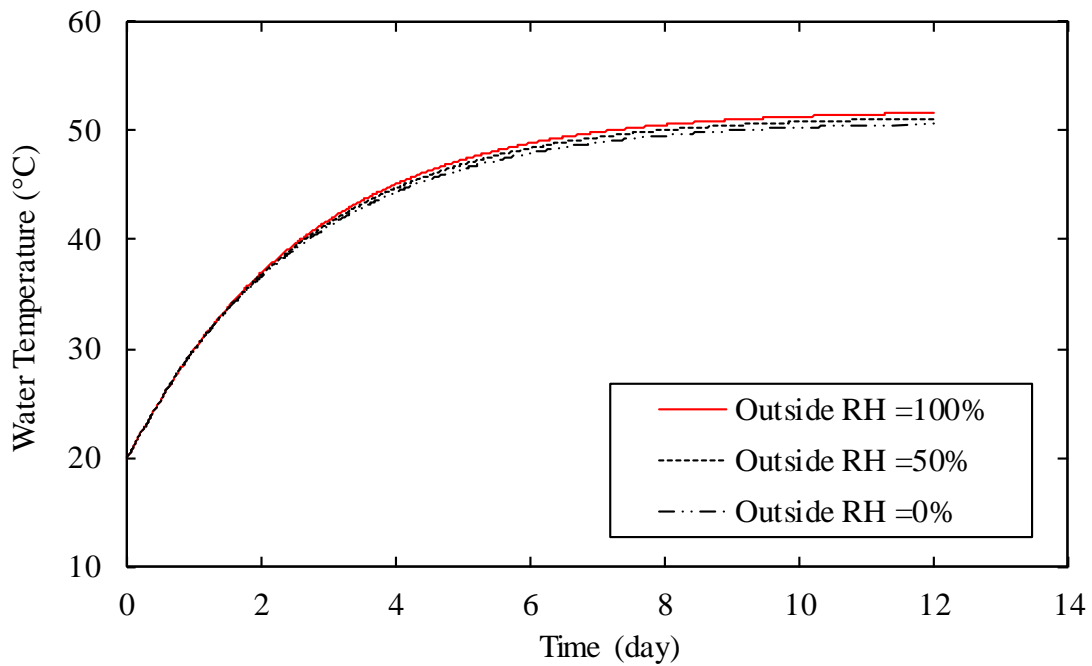


597

598 Figure 13. Effect of outside ambient air temperature on water temperature assuming 0%
 599 relative humidity.

600

601



602

603 Figure 14. Effect of the outside relative humidity on water temperature assuming an air
 604 temperature of 25 °C.

605 **6 Conclusion**

606 A Z-D model has been developed for large-scale cooling ponds. This model was validated
607 against data reported in the literature for the Maine Yankee spent fuel cooling pond. Also,
608 another validation exercise was performed to examine the applicability of the Z-D model to
609 predict the water temperature for the large-scale cooling pond. However, this validation was
610 limited to low water temperatures where validation with higher water temperatures (near 100
611 °C) has not been conducted due to the limited data available for the large-scale cooling ponds
612 and the difficulty of producing such data. It can be seen from the validation exercises that the
613 Z-D thermal model is able to predict the thermal behaviour of the cooling ponds under the
614 considered operational scenarios and with various pond sizes.

615 A number of parametric studies were performed in different situations. The first study
616 concerned the performance of the pond under normal operating conditions where the pond
617 water and air temperatures are evaluated. In the same study, the proportions of heat removal
618 components were quantified. Furthermore, a loss of cooling analysis was conducted under two
619 conditions; one without surface heat transfer and another with heat transfer. It was found that
620 the assumption leading to ignoring the heat loss from the water surface is not always a good
621 choice.

622 The last study was performed to examine the sensitivity of the pond water temperature to
623 variation in outside weather conditions. The outcomes reveal that water temperature is rather
624 insensitive to the outside relative humidity under the given scenario and the assumption of
625 constant efficiency of the cooling tower, which limits the effect of the relative humidity on the
626 cooling tower performance. On the other hand, relatively high sensitivity was observed to
627 variations in outside temperature. However, further sensitivity studies are needed to determine
628 the effect of the input parameters on the Z-D model's predictions. These studies can be
629 conducted using an appropriate statistical method in combination with the Z-D model. The Z-
630 D model will allow many studies to be performed within a reasonable time. In order to improve
631 the Z-D model, a full description of the cooling tower process need to be included.

632 **References**

- 633 [1] B. Zohuri and N. Fathi, *Thermal-hydraulic analysis of nuclear reactors*. Springer,
634 2015.
- 635 [2] W. Kuo, G. Yun, and Z. He-yi, "Spent fuel pool transient analysis under accident case
636 and the flow establishment process of passive cooling system," in *Information Systems*

- 637 *for Crisis Response and Management (ISCRAM), 2011 International Conference on,*
638 2011, pp. 482-491: IEEE.
- 639 [3] *UK Government. (September 15, 2016). Government confirms Hinkley Point C project*
640 *following new agreement in principle with EDF. Accessed 10 Januray 2017. Available:*
641 [https://www.gov.uk/government/news/government-confirms-hinkley-point-c-project-](https://www.gov.uk/government/news/government-confirms-hinkley-point-c-project-following-new-agreement-in-principle-with-edf)
642 [following-new-agreement-in-principle-with-edf](https://www.gov.uk/government/news/government-confirms-hinkley-point-c-project-following-new-agreement-in-principle-with-edf)
- 643 [4] Y. V. Kozlov, V. Safutin, N. Tikhonov, A. Tokarenko, and V. Spichev, "Long-term
644 storage and shipment of spent nuclear fuel," *Atomic Energy*, vol. 89, no. 4, pp. 792-803,
645 2000.
- 646 [5] K.-I. Ahn, J.-U. Shin, and W.-T. Kim, "Severe accident analysis of plant-specific spent
647 fuel pool to support a SFP risk and accident management," *Annals of Nuclear Energy*,
648 vol. 89, pp. 70-83, 2016.
- 649 [6] Y.-S. Chen and Y.-R. Yuann, "Accident mitigation for spent fuel storage in the upper
650 pool of a Mark III containment," *Annals of Nuclear Energy*, vol. 91, pp. 156-164, 2016.
- 651 [7] W. Fu, X. Li, X. Wu, and Z. Zhang, "Investigation of a long term passive cooling
652 system using two-phase thermosyphon loops for the nuclear reactor spent fuel pool,"
653 *Annals of Nuclear Energy*, vol. 85, pp. 346-356, 2015.
- 654 [8] J. R. Wang, H. T. Lin, Y. S. Tseng, and C. K. Shih, "Application of TRACE and CFD
655 in the spent fuel pool of Chinshan nuclear power plant," in *Applied Mechanics and*
656 *Materials*, 2012, vol. 145, pp. 78-82: Trans Tech Publ.
- 657 [9] S.-i. Tanaka, "Accident at the Fukushima Daiichi nuclear power stations of TEPCO:
658 outline & lessons learned," *Proceedings of the Japan Academy, Series B*, vol. 88, no.
659 9, pp. 471-484, 2012.
- 660 [10] R. Hasan, J. Tudor, and A. Ramadan, "Modelling of flow and heat transfer in spent fuel
661 cooling ponds," in *Proceedings of the International Congress on Advances in Nuclear*
662 *Power Plants 2015*, Nice, France.
- 663 [11] C. Ye, M. Zheng, M. Wang, R. Zhang, and Z. Xiong, "The design and simulation of a
664 new spent fuel pool passive cooling system," *Annals of Nuclear Energy*, vol. 58, pp.
665 124-131, 2013.
- 666 [12] T.-C. Hung, V. K. Dhir, B.-S. Pei, Y.-S. Chen, and F. P. Tsai, "The development of a
667 three-dimensional transient CFD model for predicting cooling ability of spent fuel
668 pools," *Applied Thermal Engineering*, vol. 50, no. 1, pp. 496-504, 2013.
- 669 [13] S. Chen, W. Lin, Y. Ferng, C. Chieng, and B. Pei, "Development of 3-D CFD
670 methodology to investigate the transient thermal-hydraulic characteristics of coolant in
671 a spent fuel pool," *Nuclear Engineering and Design*, vol. 275, pp. 272-280, 2014.
- 672 [14] C. Yanagi, M. Murase, Y. Yoshida, Y. Utanohara, T. Iwaki, and T. Nagae, "Numerical
673 Simulation of Water Temperature in a Spent Fuel Pit during the Shutdown of Its
674 Cooling Systems," *Journal of Power and Energy Systems*, vol. 6, no. 3, pp. 423-434,
675 2012.

- 676 [15] C. Yanagi, M. Murase, Y. Yoshida, T. Iwaki, T. Nagaе, and Y. Koizumi, "Evaporation
677 heat flux from hot water to air flow," *Nippon Kikai Gakkai Ronbunshu, B Hen*, vol. 78,
678 no. 786, pp. 363-372, 2012.
- 679 [16] C. Yanagi and M. Murase, "One-Region Model Predicting Water Temperature and
680 Level in a Spent Fuel Pit during Loss of All AC Power Supplies," *Journal of Power
681 and Energy Systems*, vol. 7, no. 1, pp. 18-31, 2013.
- 682 [17] C. Yanagi, M. Murase, and Y. Utanohara, "Effects of Decay Heat Distribution on Water
683 Temperature in a Spent Fuel Pit and Prediction Errors With a One-Region Model,"
684 *Journal of Nuclear Engineering and Radiation Science*, vol. 2, no. 3, p. 031001, 2016.
- 685 [18] S. Carlos, F. Sanchez-Saez, and S. Martorell, "Use of TRACE best estimate code to
686 analyze spent fuel storage pools safety," *Progress in Nuclear Energy*, vol. 77, pp. 224-
687 238, 11// 2014.
- 688 [19] V. Ognerubov, A. Kaliatka, and V. Vileiniškis, "Features of modelling of processes in
689 spent fuel pools using various system codes," *Annals of Nuclear Energy*, vol. 72, pp.
690 497-506, 2014.
- 691 [20] P. Groudev, A. Stefanova, and M. Manolov, "Investigation of dry out of SFP for
692 VVER440/V230 at Kozloduy NPP," *Nuclear Engineering and Design*, vol. 262, pp.
693 285-293, 2013.
- 694 [21] A. Kaliatka, V. Ognerubov, and V. Vileiniskis, "Analysis of the processes in spent fuel
695 pools of Ignalina NPP in case of loss of heat removal," *Nuclear Engineering and
696 Design*, vol. 240, no. 5, pp. 1073-1082, 2010.
- 697 [22] T. Watanabe, M. Ishigaki, and M. Hirano, "Analysis of BWR long-term station
698 blackout accident using TRAC-BF1," *Annals of Nuclear Energy*, vol. 49, pp. 223-226,
699 2012.
- 700 [23] X. Wu, W. Li, Y. Zhang, W. Tian, G. Su, and S. Qiu, "Analysis of the loss of pool
701 cooling accident in a PWR spent fuel pool with MAAP5," *Annals of Nuclear Energy*,
702 vol. 72, pp. 198-213, 2014.
- 703 [24] C. M. Lee and K. Lee, "A study on operation time periods of spent fuel interim storage
704 facilities in South Korea," *Progress in Nuclear Energy*, vol. 49, no. 4, pp. 323-333,
705 2007.
- 706 [25] K. A. Rogers, "Fire in the hole: A review of national spent nuclear fuel disposal policy,"
707 *Progress in Nuclear Energy*, vol. 51, no. 2, pp. 281-289, 2009.
- 708 [26] C. B. Keil, C. E. Simmons, and T. R. Anthony, *Mathematical Models for Estimating
709 Occupational Exposure to Chemicals*. American Industrial Hygiene Association, 2009.
- 710 [27] R. J. LeVeque, *Finite difference methods for ordinary and partial differential
711 equations: steady-state and time-dependent problems*. Siam, 2007.
- 712 [28] Y. Cengel, *Heat Transfer A Practical Approach*, McGraw-Hill, 2 ed. (Ellison, New
713 York). 2003, p. 609.

- 714 [29] A. C. Yunus and A. B. Michael, "Thermodynamics: An engineering approach,"
715 *McGraw-Hill, New York, 2006.*
- 716 [30] J. D. Hoffman and S. Frankel, *Numerical methods for engineers and scientists*. CRC
717 press, 2001.
- 718 [31] T. George, S. Claybrook, L. Wiles, and C. Wheeler, "GOTHIC Containment Analysis
719 Package, User Manual, Version 7.2 b, NAI 8907-02 Rev 18," 2009.
- 720